HHS Public Access

Author manuscript

Science. Author manuscript; available in PMC 2018 November 19.

Published in final edited form as:

Science. 2018 May 04; 360(6388): 508–513. doi:10.1126/science.aas9466.

Activation mechanism of a human SK-calmodulin channel complex elucidated by cryo-EM structures

Chia-Hsueh Lee and **Roderick MacKinnon***

Laboratory of Molecular Neurobiology and Biophysics, The Rockefeller University, Howard Hughes Medical Institute, 1230 York Avenue, New York, New York 10065, USA.

Abstract

Small-conductance Ca^{2+}-activated K^+ (SK) channels mediate neuron excitability and are associated with synaptic transmission and plasticity. They also regulate immune responses and the size of blood cells. Activation of SK channels requires calmodulin (CaM), but how CaM binds and opens SK channels has been unclear. Here we report cryo-electron microscopy (cryo-EM) structures of a human SK4-CaM channel complex in closed and activated states at 3.4- and 3.5-angstrom resolution, respectively. Four CaM molecules bind to one channel tetramer. Each lobe of CaM serves a distinct function: The C-lobe binds to the channel constitutively, whereas the N-lobe interacts with the S4–S5 linker in a Ca^{2+}-dependent manner. The S4–S5 linker, which contains two distinct helices, undergoes conformational changes upon CaM binding to open the channel pore. These structures reveal the gating mechanism of SK channels and provide a basis for understanding SK channel pharmacology.

Introduction

Ca^{2+} is arguably one of the most crucial cellular signals, and it affects virtually every aspect of a cell. Gárdos first discovered a link between Ca^{2+} and K^+ permeability in 1958 when he recognized that Ca^{2+} can enhance the K^+ permeability of human erythrocytes (1). Since then, several studies have reported a similar “Gárdos effect” in various types of neurons (2). We now know that this effect is mediated by a family of Ca^{2+}-activated K^+ channels (3). These channels were historically cataloged as intermediate- or small-conductance Ca^{2+}-activated K^+ (SK) channels to distinguish them from the well-studied large-conductance Ca^{2+}-activated K^+ (BK) channels (4–8). Widely expressed in neurons of the central nervous system, SK channels contribute to the after-hyperpolarization following an action potential and mediate the intrinsic excitability of neurons (9). SK channels are also implicated in synaptic transmission and plasticity. In T lymphocytes, SK channels modulate the activation

*Correspondence to: mackinn@rockefeller.edu.

Author contributions: C-H.L. performed all experiments. C-H.L. and R.M. analyzed the structures and wrote the manuscript.

Competing interests: The authors declare no competing financial interests.

Data and materials availability: Cryo-EM density maps of the SK-CaM complex have been deposited in the Electron Microscopy Data Bank under accession codes EMD-7537 (Ca^{2+}-free state), 7538 (Ca^{2+}-bound state I) and 7539 (Ca^{2+}-bound state II). Atomic coordinates have been deposited in the Protein Data Bank under accession codes 6CNM (Ca^{2+}-free state), 6CNN (Ca^{2+}-bound state I), and 6CNO (Ca^{2+}-bound state II).

of immune responses (7, 10, 11). In erythrocytes, they regulate cell volume, and their dysfunction causes cell dehydration and hemolysis (8, 12–15).

Given the physiological importance of SK channels, it is important to understand how they work at a molecular level. Although both SK and BK channels are activated by Ca^{2+}, their amino acid sequence identities are low, and their channel gating mechanisms are completely different. Ca^{2+} ions open BK channels directly, whereas Ca^{2+} ions open SK channels via calmodulin (CaM) (4, 16). CaM opens SK channels in a cooperative manner with high Ca^{2+} sensitivity (median effective concentration, around 100 to 400 nM) (4–7, 17). The structures of BK channels have been studied in molecular detail (18, 19), but the Ca^{2+}-CaM gating mechanism of SK channels has remained a mystery. To understand the structural basis of gating in SK channels, we determined structures of a full-length human SK channel in closed and activated states by using single-particle cryo-electron microscopy (cryo-EM).

Results

Characterization of a human SK4-CaM channel complex

After an initial screening of 25 SK proteins from different species by fluorescence-detection size-exclusion chromatography (20), we identified human SK4 (also known as IK, $K_{Ca}3.1$, *KCNN4*, or Gárdos channel) as a promising candidate for structural studies. We then expressed and purified human SK4 from mammalian cells. Purified full-length SK4 channels, although having a predicted molecular mass of 48 kDa, migrate at about 37 kDa SDS–polyacrylamide gel electrophoresis (SDS-PAGE) (Fig. 1A). CaM was copurified with the channel in both the presence and absence of Ca^{2+}. This observation suggests that Ca^{2+} is not necessary for the SK-CaM interaction and that CaM constitutively binds to the channel.

To examine the function of the purified SK4-CaM complex, we reconstituted it into liposomes and monitored K^+ flux by means of a fluorescence-based assay (21). Proteoliposomes were reconstituted with a high concentration of K^+ (150 mM KCl), then diluted into K^+-free solution while ionic strength was maintained with 150 mM NaCl. In the presence of Ca^{2+}, a fluorescence decrease was observed owing to K^+ efflux out of the liposomes (Fig. 1A), which could be inhibited using two different SK4 channel blockers, NS6180 and senicapoc (22, 23). Thus, the purified SK4-CaM protein complex (hereafter referred to as SK-CaM) recapitulates the functional Ca^{2+}-activated K^+ efflux and pharmacological inhibition characteristic of native channels.

Architecture of Ca^{2+}-free SK-CaM channel complex

We first determined the structure of SK-CaM in the absence of Ca^{2+} to a resolution of 3.4 Å (figs. S1 and S2). We found that four SK subunits form a fourfold-symmetric tetramer that is ~95 Å in length and 120 Å in width when viewed from within the plane of the membrane (Fig. 1B). Transmembrane helices S5 and S6 form the ion channel pore, which is surrounded by membrane-embedded helices S1 to S4. The domain comprising these four helices interacts with the pore domain from the same subunit (Fig. 1C). This arrangement is similar to that of the BK channel (also known as Slo1) but different from that of domain-swapped

K_v1 to K_v7 channels, where helices S1 to S4 interact with a neighboring pore domain (18, 24, 25).

At the C-terminal end of S6, the helix unwinds near the inner leaflet of the cell membrane. This allows the polypeptide to make a sharp turn before two helices, HA and HB, that run almost parallel to the membrane plane. HB is followed by the HC helix (Fig. 1D). The HC helices from four SK subunits make up a coiled coil located at the center of the channel, which is important for channel assembly and trafficking (26, 27). Because this region of the channel is flexible, the local structure is not as well resolved as other regions, and the last 41 residues are invisible in the structure. Consistent with previous studies (28, 29), the peripheral ends of HA and HB form the binding site for the CaM C-lobes, which are visible in the cryo-EM map (Fig. 1D). On the basis of light scattering and analytical ultracentrifugation experiments performed on CaMs and channel fragments, Halling et al. suggested that two to eight CaM molecules may bind to one channel (30). In the context of a full-length channel, we observed that one CaM binds to one SK subunit, resulting in four CaMs per channel tetramer.

Dynamic CaM N-lobe as a Ca^{2+} sensor

When *C*4 symmetry was imposed during cryo-EM reconstruction, the CaM N-lobes of the channel complex exhibited poor density, which precluded model building of this portion of CaM (Fig. 1, B to D, and fig. S1C). This suggests that the N-lobes exhibit static disorder, consistent with high mobility in the absence of Ca^{2+}. When the structure was reconstructed without imposing symmetry, only one of the four CaM N-lobes was visible (fig. S1C). To analyze the static disorder of the CaM N-lobes further, we expanded the data set and reoriented each subunit onto a single position according to the *C*4 point group (31). We then performed focused classification and subsequent refinement (fig. S3A). Through this strategy, three distinct conformations of CaM with improved N-lobe density were identified (Fig. 2).

In these reconstructions, the differences in the CaM C-lobes are subtle, resulting from a slight sliding along the HA and HB helices (fig. S3, B and C). In contrast, the CaM N-lobes exhibit large positional variations. It is evident that the N-lobe can swing from the periphery of the channel (Fig. 2, red) all the way to the center of the channel, close to the coiled coil (Fig. 2, blue). The N- and C-lobes of CaM are connected by a central linker, which has the capacity to maintain an α-helical structure or unwind into a loop, allowing CaM to adopt multiple conformations (32). Under Ca^{2+}-free conditions in SK-CaM, this flexible linker permits the N-lobe to undergo long-range, rigid-body-like motions, traveling from the bottom of the S2 helix to the bottom of the S4–S5 linker (Figs. 2B and 1D), while the C-lobe maintains its interaction with the HA and HB helices (fig. S3C). Previous mutagenesis experiments suggested that the two lobes of CaM serve distinct functions in the SK channel complex (33–35): The C-lobe interacts with SK channels in a Ca^{2+}-independent manner, whereas the N-lobe senses Ca^{2+} and gates the channel. Our structure supports these findings by demonstrating a permanent bound CaM C-lobe and a dynamic N-lobe. This molecular plasticity of the N-lobe seems ideal for rapid detection and response to local Ca^{2+} signals.

Transmembrane domain and ion conduction pore

Although the SK channel has a similar topology to the BK channel, we noticed two interesting differences. First, the S1 and S2 helices in SK are much longer than those in BK (18). Each about 60 Å in length, S1 and S2 in SK extend beyond the membrane boundary, into the cytoplasmic space (Fig. 3A). The second difference involves the S4–S5 linker, which in SK consists of two α-helices, $S_{45}A$ and $S_{45}B$, rather than the short turn observed in BK and other non-domain-swapped members of the six-transmembrane ion channel superfamily, including the K_v10 to K_v12, Slo2, and HCN channels (18, 36–39). In voltage-gated ion channels — whether domain-swapped or not — the S4–S5 linker plays a critical role in channel gating by coupling movements of the voltage sensor to opening of the pore. But SK is voltage-insensitive (5, 6, 17). Its particular S4–S5 linker structure is apparently suited to confer CaM-mediated Ca^{2+} sensitivity to the SK channel gate.

$S_{45}B$ is wedged in between HA and S6, thus providing lateral contacts between the pore and the cytoplasmic structural elements that ultimately attach CaM to the channel (Fig. 3B). Hydrogen bonds formed between Lys197 on $S_{45}B$ and Glu295 on HA from a neighboring subunit, and between Asn201 on $S_{45}B$ and Arg287 on S6 from the same subunit, appear to "glue" these structural elements together. Mutations of Arg287, possibly by interfering with this interaction, change the intrinsic open probability of SK channels in the absence of Ca^{2+} (40). The inter-subunit connectivity of this interface (each S4–S5 linker interacts structurally with S6 from two subunits) could be the structural underpinning of the high cooperativity of Ca^{2+} activation in SK (4–7, 17).

In the absence of Ca^{2+} the SK channel is functionally closed. The structure, determined in the absence of Ca^{2+} also appears closed. Residues Val282 from each of the four S6 helices form a constricted gate with radius less than 1 Å (Fig. 3C). This finding is in good agreement with studies that have used thiol-reactive methanethiosulfonate (MTS) reagents to assess the reactivity of site-directed cysteine residues placed along the S6 helix (41–44). Furthermore, it has been shown that replacement of Val282 by Gly produces a "leaky" channel that conducts current in the absence of Ca^{2+} (45). The structure also provides information on the molecular basis of the channelopathy known as hereditary xerocytosis, a type of hemolytic anemia associated with human SK4 mutations Val282Glu and Val282Met (14, 15, 46, 47). These two gain-of-function mutations involve precisely that residue which forms the narrowest constriction within the pore of the closed SK channel.

Structures of Ca^{2+}-bound SK-CaM channel complex

To visualize an open conformation and understand how Ca^{2+} activation occurs, we determined the structure of the SK-CaM complex in the presence of Ca^{2+} to a resolution of 3.5 Å (figs. S4 and S5). We again observed that four CaMs bind to a channel tetramer (Fig. 4, A and B), just as in the Ca^{2+}-free state. However, the density for the CaM N-lobe was significantly improved relative to that in the Ca^{2+}-free structure., permitting the building of an entire CaM model. Ca^{2+} binding alters the conformation of the CaM N-lobe and causes it to attach firmly to the channel. The structure reveals several previously unidentified interactions between Ca^{2+}-bound CaM and the channel subunits. First, cytosolic portions of the S1 and S2 helices, which extend into the cytoplasmic space, directly contact CaM (Fig.

4, C and D). Such interactions provide a plausible justification for the extraordinary length of S1 and S2. Second, the N-lobe interacts with HA and HC from an adjacent subunit (Fig. 4, C and D, yellow subunit). Through these newly formed interactions, Ca^{2+}-bound CaM and the SK channel form an extensive interaction network, with each CaM molecule communicating with three channel subunits (Fig. 4, C and D, green, blue, and yellow subunits). This distributed interaction could potentially permit conformational changes brought about through the binding of one CaM N-lobe to influence the neighboring CaM molecules. It seems likely that this structural property could give rise, at least in part, to the high cooperativity that is characteristic of SK channel activation.

Two major differences between the full-length cryo-EM structure and the previously determined crystal structure of CaM in complex with channel fragments (HA, HB, and part of HC) (29) deserve attention. First, in the cryo-EM structure, the CaM N-lobe binding pocket recognizes $S_{45}A$, the first helix of the S4–S5 linker (Fig. 4, C and D), whereas in the crystal structure, the N-lobe binds to HC rather than $S_{45}A$ ($S_{45}A$ was not included in the crystallization construct). Many of the residues forming the HC binding site in the crystal structure are buried at the center of the coiled coil in the cryo-EM structure (fig. S6). The buried residues are therefore likely not accessible to the CaM N-lobe in the full-length channel. We conclude that $S_{45}A$ is the functional CaM N-lobe binding site.

Second, in the crystal structure the channel fragments and CaMs form a dimeric, twofold-symmetric structure. On the basis of that observation, a mechanism was proposed in which channel activation breaks down the fourfold symmetry, causing the channel to become a twofold-symmetric dimer-of-dimers. This transition was proposed to generate a rotary force to open the channel (29). Although this was a reasonable idea given the structures of channel fragments, the full-length structure shows that the activated SK-CaM complex remains fourfold-symmetric throughout (Fig. 4, A and B, and fig. S4C).

Structural basis for channel activation

Although the amino acid sequence of $S_{45}A$ does not correspond to a known canonical CaM-binding motif (48), $S_{45}A$ is highly conserved, and residues directly facing the CaM N-lobe pocket (Ala, Ser, and Leu) are identical across the SK channel family (Fig. 5A), suggesting that this region is crucial to channel function. When the CaM N-lobe binds, it pulls the $S_{45}A$ helix downward and displaces it by 4 Å (as measured at the C-terminal end of $S_{45}A$) (Fig. 5B, activated state I). This in turn causes $S_{45}B$ to move outward, away from the pore axis. Because $S_{45}B$ is tightly coupled to the pore-lining S6 helix (Fig. 3B), this displacement of $S_{45}B$ expands the S6 helical bundle and enlarges the radius of the cytoplasmic pore entrance to 5 Å (Fig. 5, B and D). In addition, the channel gate formed by Val282 expands. Even after this expansion, the Val282 side chain still constricts the pore to a radius of ~1.6 Å (Fig. 5, C and D), which is too narrow to permit the flow of hydrated K^+ ions. In this activated state I, the channel is undergoing movements toward opening, although the pore appears to remain non-conductive. The existence of such a channel conformation is supported by functional studies, which indicate that the maximum channel-open probability of SK4 remains low (49, 50), usually 0.1 to 0.3, at saturating concentrations of Ca^{2+}. Thus, even under maximal stimulation, the channel is still more often in a non-conductive conformation.

Through three-dimensional classification, we identified another activated state (Fig. 5, B to D, activated state II) and determined the corresponding structure at moderate resolution (4.7 Å) (figs. S4C and S7). Compared with activated state I, the CaM N-lobe binding more dramatically rearranges $S_{45}A$, $S_{45}B$, and S6 in state II. $S_{45}A$ and $S_{45}B$ are displaced by an additional 2 Å (Fig. 5B, and fig. S7D), which causes S6 to move further away from the pore axis. This expands the channel gate at the level of Val282 to a radius of ~3.5 Å (Fig. 5, C and D), which would allow permeation of partially hydrated K^+ ions. State II is less populated than state I (fig. S4C), which is consistent with open probability measurements showing that activated channels occupy a conductive state with lower probability than they occupy the non-conductive states. These analyses reinforce the notion that activated state II likely represents an open, conductive state of SK channels, although future higher-resolution structures will be required to reach an unambiguous conclusion.

Our structures lead us to propose that the binding of the CaM N-lobe to $S_{45}A$ initiates channel activation. This proposal predicts that preventing the interaction between CaM and $S_{45}A$ would preclude channel opening. To test this prediction, we introduced a cysteine at position 181 on the $S_{45}A$ helix. Ser181 is located in the middle of $S_{45}A$ and points directly into the CaM N-lobe pocket. We reasoned that labeling this position with a negative-charged MTS reagent (MTSES) would reduce the affinity of the CaM N-lobe and thereby impede N-lobe binding (Fig. 5E). After exposure to MTSES, the current from the Ser181Cys mutant channels diminished significantly (7 ± 7% remaining current), whereas the current from wild-type channels showed only a small reduction (81 ± 9% remaining current). These results support the proposed role of the CaM N-lobe–$S_{45}A$ interaction in channel gating.

Discussion

On the basis of the structural and functional analyses presented here, we propose a new model for SK channel activation (Fig. 6). In the absence of Ca^{2+}, CaM pre-associates with the channel through its C-lobe. Meanwhile, the CaM N-lobe maintains only weak interactions with the channel and is conformationally flexible. In this resting state, the channel pore is closed. In the presence of increasing Ca^{2+} concentrations, the CaM N-lobe binds to Ca^{2+}. This triggers a conformational change, which increases the affinity of the N-lobe for the $S_{45}A$ helix within the S4–S5 linker. Upon CaM binding, $S_{45}A$ is displaced downward (towards the cytoplasm), which causes $S_{45}B$ to move away from the pore axis. Such a movement rearranges the S6 helices, permitting the pore to open. As an aid to visualizing the structural transition of SK channel activation, we animated the CaM movement and the corresponding conformational changes in the SK channel upon Ca^{2+} binding. This animation illustrates how CaM opens the SK channel and encapsulates the activation model (movie S1).

Several studies have shown that the phosphorylation state of CaM regulates SK channel activity (51–53). When CaM is phosphorylated at position Thr79, the apparent Ca^{2+} sensitivity of the SK channel is reduced, causing the channel to close more rapidly (52). One hypothesis to explain this is that Thr79 phosphorylation disrupts interactions between lipids and the SK-CaM complex (53). Our study provides a basis for interpreting these functional studies and perhaps for building on the hypothesis. Thr79 is positioned within the hinge that

connects the CaM N- and C-lobes, which is wedged between S2 and HB and faces toward the lipid membrane (Fig. 4, C and D). The addition of a phosphate group to Thr79 would seem likely to influence the conformation of the surrounding channel subunits and/or influence lipid-channel interactions.

Riluzole, the first U.S. Food and Drug Administration-approved medication for amyotrophic lateral sclerosis, has been suggested to act through SK channels (54, 55). Riluzole and related compounds (e.g., 1-EBIO) potentiate SK channel activity and are proposed, on the basis of crystal structures, to bind to the interface between the CaM N-lobe and HC (56–59). Because our results redefine the native CaM N-lobe binding interface, we suggest that SK channel potentiators may instead bind in between the CaM N-lobe and $S_{45}A$ (fig. S8). Such a possibility needs further exploration.

This study provides a plausible mechanism of SK channel activation and highlights the role of the S4–S5 linker in coupling Ca^{2+}-induced CaM binding to channel opening. Our structures also provide a foundation for the development of therapeutic agents targeting SK channels.

Supplementary Material

Refer to Web version on PubMed Central for supplementary material.

Acknowledgments:

We thank M. Ebrahim and J. Sotiris at the Evelyn Gruss Lipper Cryo-EM Resource Center of Rockefeller University for assistance with data collection and members of the MacKinnon and Jue Chen laboratories for helpful discussions. We gratefully acknowledge the support of NVIDIA Corporation with the donation of the Titan X Pascal GPU used for this research.

Funding: This work was supported in part by National Institutes of Health grant GM43949. C-H.L. is supported by the Jane Coffin Childs Memorial Fund fellowship (#61-1632). R.M. is an investigator of the Howard Hughes Medical Institute.

References and Notes:

1. Gárdos G, The function of calcium in the potassium permeability of human erythrocytes. Biochim. Biophys. Acta 30, 653–4 (1958). [PubMed: 13618284]
2. Adelman JP, SK channels and calmodulin. Channels (Austin) 10, 1–6 (2016).
3. Kaczmarek LK et al., International Union of Basic and Clinical Pharmacology. C. Nomenclature and Properties of Calcium-Activated and Sodium-Activated Potassium Channels. Pharmacol. Rev 69, 1–11 (2017). [PubMed: 28267675]
4. Xia XM et al., Mechanism of calcium gating in small-conductance calcium-activated potassium channels. Nature 395, 503–7 (1998). [PubMed: 9774106]
5. Ishii TM et al., A human intermediate conductance calcium-activated potassium channel. Proc. Natl. Acad. Sci. U. S. A 94, 11651–6 (1997). [PubMed: 9326665]
6. Joiner WJ, Wang L-YY, Tang MD, Kaczmarek LK, hSK4, a member of a novel subfamily of calcium-activated potassium channels. Proc. Natl. Acad. Sci. U. S. A 94, 11013–8 (1997). [PubMed: 9380751]
7. Logsdon NJ, Kang J, Togo JA, Christian EP, Aiyar J, A novel gene, hKCa4, encodes the calcium-activated potassium channel in human T lymphocytes. J. Biol. Chem 272, 32723–6 (1997). [PubMed: 9407042]

8. Vandorpe DH et al., cDNA cloning and functional characterization of the mouse Ca2+-gated K+ channel, mIK1. Roles in regulatory volume decrease and erythroid differentiation. J. Biol. Chem 273, 21542–53 (1998). [PubMed: 9705284]
9. Adelman JP, Maylie J, Sah P, Small-conductance Ca2+-activated K+ channels: form and function. Annu. Rev. Physiol 74, 245–69 (2012). [PubMed: 21942705]
10. Cahalan MD, Chandy KG, The functional network of ion channels in T lymphocytes. Immunol. Rev 231, 59–87 (2009). [PubMed: 19754890]
11. Feske S, Wulff H, Skolnik EY, Ion channels in innate and adaptive immunity. Annu. Rev. Immunol 33, 291–353 (2015). [PubMed: 25861976]
12. Hoffman JF et al., The hSK4 (KCNN4) isoform is the Ca2+-activated K+ channel (Gardos channel) in human red blood cells. Proc. Natl. Acad. Sci. U. S. A 100, 7366–71 (2003). [PubMed: 12773623]
13. Rapetti-Mauss R et al., A mutation in the Gardos channel is associated with hereditary xerocytosis. Blood 126, 1273–80 (2015). [PubMed: 26148990]
14. Glogowska E, Lezon-Geyda K, Maksimova Y, Schulz VP, Gallagher PG, Mutations in the Gardos channel (KCNN4) are associated with hereditary xerocytosis. Blood 126, 1281–4 (2015). [PubMed: 26198474]
15. Andolfo I et al., Novel Gardos channel mutations linked to dehydrated hereditary stomatocytosis (xerocytosis). Am. J. Hematol 90, 921–6 (2015). [PubMed: 26178367]
16. Fanger CM et al., Calmodulin mediates calcium-dependent activation of the intermediate conductance KCa channel, IKCa1. J. Biol. Chem 274, 5746–54 (1999). [PubMed: 10026195]
17. Köhler M et al., Small-conductance, calcium-activated potassium channels from mammalian brain. Science 273, 1709–14 (1996). [PubMed: 8781233]
18. Tao X, Hite RK, MacKinnon R, Cryo-EM structure of the open high-conductance Ca2+-activated K+ channel. Nature 541, 46–51 (2016). [PubMed: 27974795]
19. Hite RK, Tao X, MacKinnon R, Structural basis for gating the high-conductance Ca2+-activated K + channel. Nature 541, 52–57 (2017). [PubMed: 27974801]
20. Kawate T, Gouaux E, Fluorescence-detection size-exclusion chromatography for precrystallization screening of integral membrane proteins. Structure 14, 673–681 (2006). [PubMed: 16615909]
21. Su Z, Brown EC, Wang W, MacKinnon R, Novel cell-free high-throughput screening method for pharmacological tools targeting K+ channels. Proc. Natl. Acad. Sci. U. S. A 113, 5748–53 (2016). [PubMed: 27091997]
22. Strøbæk D et al., NS6180, a new K(Ca) 3.1 channel inhibitor prevents T-cell activation and inflammation in a rat model of inflammatory bowel disease. Br. J. Pharmacol 168, 432–44 (2013). [PubMed: 22891655]
23. Stocker JW et al., ICA-17043, a novel Gardos channel blocker, prevents sickled red blood cell dehydration in vitro and in vivo in SAD mice. Blood 101, 2412–8 (2003). [PubMed: 12433690]
24. Long SB, Campbell EB, Mackinnon R, Crystal structure of a mammalian voltage-dependent Shaker family K+ channel. Science 309, 897–903 (2005). [PubMed: 16002581]
25. Sun J, MacKinnon R, Cryo-EM Structure of a KCNQ1/CaM Complex Reveals Insights into Congenital Long QT Syndrome. Cell 169, 1042–1050.e9 (2017). [PubMed: 28575668]
26. Syme CA et al., Trafficking of the Ca2+-activated K+ channel, hIK1, is dependent upon a C-terminal leucine zipper. J. Biol. Chem 278, 8476–86 (2003). [PubMed: 12493744]
27. Tuteja D et al., Cardiac small conductance Ca2+-activated K+ channel subunits form heteromultimers via the coiled-coil domains in the C termini of the channels. Circ. Res 107, 851–9 (2010). [PubMed: 20689065]
28. Wissmann R et al., A helical region in the C terminus of small-conductance Ca2+-activated K+ channels controls assembly with apo-calmodulin. J. Biol. Chem 277, 4558–64 (2002). [PubMed: 11723128]
29. Schumacher MA, Rivard AF, Bächinger HP, Adelman JP, Structure of the gating domain of a Ca2+-activated K+ channel complexed with Ca2+/calmodulin. Nature 410, 1120–4 (2001). [PubMed: 11323678]

30. Halling DB, Kenrick SA, Riggs AF, Aldrich RW, Calcium-dependent stoichiometries of the KCa2.2 (SK) intracellular domain/calmodulin complex in solution. J. Gen. Physiol 143, 231–52 (2014). [PubMed: 24420768]

31. Scheres SHW, Processing of Structurally Heterogeneous Cryo-EM Data in RELION. Methods Enzymol 579, 125–57 (2016). [PubMed: 27572726]

32. Tidow H, Nissen P, Structural diversity of calmodulin binding to its target sites. FEBS J 280, 5551–5565 (2013). [PubMed: 23601118]

33. Keen JE et al., Domains responsible for constitutive and Ca(2+)-dependent interactions between calmodulin and small conductance Ca(2+)-activated potassium channels. J. Neurosci 19, 8830–8 (1999). [PubMed: 10516302]

34. Lee W-S, Ngo-Anh TJ, Bruening-Wright A, Maylie J, Adelman JP, Small conductance Ca2+-activated K+ channels and calmodulin: cell surface expression and gating. J. Biol. Chem 278, 25940–6 (2003). [PubMed: 12734181]

35. Li W, Halling DB, Hall AW, Aldrich RW, EF hands at the N-lobe of calmodulin are required for both SK channel gating and stable SK-calmodulin interaction. J. Gen. Physiol 134, 281–93 (2009). [PubMed: 19752189]

36. Hite RK, MacKinnon R, Structural Titration of Slo2.2, a Na+-Dependent K+ Channel. Cell 168, 390–399.e11 (2017). [PubMed: 28111072]

37. Whicher JR, MacKinnon R, Structure of the voltage-gated K+ channel Eag1 reveals an alternative voltage sensing mechanism. Science 353, 664–9 (2016). [PubMed: 27516594]

38. Wang W, MacKinnon R, Cryo-EM Structure of the Open Human Ether-à-go-go-Related K+ Channel hERG. Cell 169, 422–430.e10 (2017). [PubMed: 28431243]

39. Lee C-H, MacKinnon R, Structures of the Human HCN1 Hyperpolarization-Activated Channel. Cell 168, 111–120.e11 (2017). [PubMed: 28086084]

40. Li W, Aldrich RW, Electrostatic influences of charged inner pore residues on the conductance and gating of small conductance Ca2+ activated K+ channels. Proc. Natl. Acad. Sci. U. S. A 108, 5946–53 (2011). [PubMed: 21422289]

41. Simoes M et al., Cysteine mutagenesis and computer modeling of the S6 region of an intermediate conductance IKCa channel. J. Gen. Physiol 120, 99–116 (2002). [PubMed: 12084779]

42. Bruening-Wright A, Schumacher MA, Adelman JP, Maylie J, Localization of the activation gate for small conductance Ca2+-activated K+ channels. J. Neurosci 22, 6499–506 (2002). [PubMed: 12151529]

43. Klein H et al., Structural determinants of the closed KCa3.1 channel pore in relation to channel gating: results from a substituted cysteine accessibility analysis. J. Gen. Physiol 129, 299–315 (2007). [PubMed: 17353352]

44. Bruening-Wright A, Lee W-S, Adelman JP, Maylie J, Evidence for a deep pore activation gate in small conductance Ca2+-activated K+ channels. J. Gen. Physiol 130, 601–10 (2007). [PubMed: 17998394]

45. Garneau L et al., Hydrophobic interactions as key determinants to the KCa3.1 channel closed configuration. An analysis of KCa3.1 mutants constitutively active in zero Ca2+. J. Biol. Chem 284, 389–403 (2009). [PubMed: 18996847]

46. Rapetti-Mauss R, Soriani O, Vinti H, Badens C, Guizouarn H, Senicapoc: a potent candidate for the treatment of a subset of hereditary xerocytosis caused by mutations in the Gardos channel. Haematologica 101, e431–e435 (2016). [PubMed: 27443288]

47. Rivera A et al., Erythrocytes from hereditary xerocytosis patients heterozygous for KCNN4 V282M exhibit increased spontaneous Gardos channel-like activity inhibited by senicapoc. Am. J. Hematol 92, E108–E110 (2017). [PubMed: 28295477]

48. Mruk K, Farley BM, Ritacco AW, Kobertz WR, Calmodulation meta-analysis: predicting calmodulin binding via canonical motif clustering. J. Gen. Physiol 144, 105–14 (2014). [PubMed: 24935744]

49. Jones HM et al., An NH2-terminal multi-basic RKR motif is required for the ATP-dependent regulation of hIK1. Channels (Austin) 1, 80–91 (2007). [PubMed: 18690018]

50. Morales P et al., Contribution of the KCa3.1 channel–calmodulin interactions to the regulation of the KCa3.1 gating process. J. Gen. Physiol (2013), doi:10.1085/jgp.201210933.

51. Bildl W et al., Protein kinase CK2 is coassembled with small conductance Ca(2+)-activated K+ channels and regulates channel gating. Neuron 43, 847–58 (2004). [PubMed: 15363395]
52. Allen D, Fakler B, Maylie J, Adelman JP, Organization and regulation of small conductance Ca2+-activated K+ channel multiprotein complexes. J. Neurosci 27, 2369–76 (2007). [PubMed: 17329434]
53. Zhang M et al., Selective phosphorylation modulates the PIP2 sensitivity of the CaM-SK channel complex. Nat. Chem. Biol 10, 753–9 (2014). [PubMed: 25108821]
54. Cao Y-J, Dreixler JC, Couey JJ, Houamed KM, Modulation of recombinant and native neuronal SK channels by the neuroprotective drug riluzole. Eur. J. Pharmacol 449, 47–54 (2002). [PubMed: 12163105]
55. Dimitriadi M et al., The neuroprotective drug riluzole acts via small conductance Ca2+-activated K + channels to ameliorate defects in spinal muscular atrophy models. J. Neurosci 33, 6557–62 (2013). [PubMed: 23575853]
56. Zhang M, Pascal JM, Schumann M, Armen RS, Zhang J-F, Identification of the functional binding pocket for compounds targeting small-conductance Ca2+-activated potassium channels. Nat. Commun 3, 1021 (2012). [PubMed: 22929778]
57. Zhang M, Pascal JM, Zhang J-F, Unstructured to structured transition of an intrinsically disordered protein peptide in coupling Ca2+-sensing and SK channel activation. Proc. Natl. Acad. Sci. U. S. A 110, 4828–33 (2013). [PubMed: 23487779]
58. Brown BM, Shim H, Zhang M, Yarov-Yarovoy V, Wulff H, Structural Determinants for the Selectivity of the Positive KCa3.1 Gating Modulator 5-Methylnaphtho[2,1-d]oxazol-2-amine (SKA-121). Mol. Pharmacol 92, 469–480 (2017). [PubMed: 28760780]
59. Nam Y-W et al., Structural insights into the potency of SK channel positive modulators. Sci. Rep 7, 17178 (2017). [PubMed: 29214998]
60. Zhang M, Tanaka T, Ikura M, Calcium-induced conformational transition revealed by the solution structure of apo calmodulin. Nat. Struct. Biol 2, 758–67 (1995). [PubMed: 7552747]
61. Kuboniwa H et al., Solution structure of calcium-free calmodulin. Nat. Struct. Biol 2, 768–76 (1995). [PubMed: 7552748]
62. Goehring A et al., Screening and large-scale expression of membrane proteins in mammalian cells for structural studies. Nat. Protoc 9, 2574–85 (2014). [PubMed: 25299155]
63. Weissmann F et al., biGBac enables rapid gene assembly for the expression of large multisubunit protein complexes. Proc. Natl. Acad. Sci. U. S. A 113, E2564–9 (2016). [PubMed: 27114506]
64. Kirchhofer A et al., Modulation of protein properties in living cells using nanobodies. Nat. Struct. Mol. Biol 17, 133–138 (2010). [PubMed: 20010839]
65. Mastronarde DN, Automated electron microscope tomography using robust prediction of specimen movements. J. Struct. Biol 152, 36–51 (2005). [PubMed: 16182563]
66. Zheng SQ et al., MotionCor2: anisotropic correction of beam-induced motion for improved cryo-electron microscopy. Nat. Methods 14, 331–332 (2017). [PubMed: 28250466]
67. Zhang K, Gctf: Real-time CTF determination and correction. J. Struct. Biol 193, 1–12 (2016). [PubMed: 26592709]
68. Scheres SHW, RELION: implementation of a Bayesian approach to cryo-EM structure determination. J. Struct. Biol 180, 519–30 (2012). [PubMed: 23000701]
69. Punjani A, Rubinstein JL, Fleet DJ, Brubaker MA, cryoSPARC: algorithms for rapid unsupervised cryo-EM structure determination. Nat. Methods 14, 290–296 (2017). [PubMed: 28165473]
70. Bai X, Rajendra E, Yang G, Shi Y, Scheres SH, Sampling the conformational space of the catalytic subunit of human γ-secretase. Elife 4, e11182 (2015). [PubMed: 26623517]
71. Scheres SHW, Beam-induced motion correction for sub-megadalton cryo-EM particles. Elife 3, e03665 (2014). [PubMed: 25122622]
72. Chen S et al., High-resolution noise substitution to measure overfitting and validate resolution in 3D structure determination by single particle electron cryomicroscopy. Ultramicroscopy 135, 24–35 (2013). [PubMed: 23872039]
73. Scheres SHW, Chen S, Prevention of overfitting in cryo-EM structure determination. Nat. Methods 9, 853–4 (2012). [PubMed: 22842542]

74. Emsley P et al., Features and development of Coot. Acta Crystallogr. Sect. D Biol. Crystallogr 66, 486–501 (2010). [PubMed: 20383002]

75. Pettersen EF et al., UCSF Chimera--a visualization system for exploratory research and analysis. J. Comput. Chem 25, 1605–12 (2004). [PubMed: 15264254]

76. V Afonine P, Headd JJ, Terwilliger TC, Adams PD, New tool: phenix. real_space_refine. Comput. Crystallogr. Newsl 4, 43–44 (2013).

77. Chen VB et al., MolProbity: All-atom structure validation for macromolecular crystallography. Acta Crystallogr. Sect. D Biol. Crystallogr 66, 12–21 (2010). [PubMed: 20057044]

78. Barad BA et al., EMRinger: side chain–directed model and map validation for 3D cryo-electron microscopy. Nat. Methods 12, 943–946 (2015). [PubMed: 26280328]

79. Smart OS, Neduvelil JG, Wang X, Wallace BAA, Sansom MSP, HOLE: a program for the analysis of the pore dimensions of ion channel structural models. J. Mol. Graph 14, 354–360 (1996). [PubMed: 9195488]

80. Schrödinger LLC, The PyMOL Molecular Graphics System, Version 2.0 (2017).

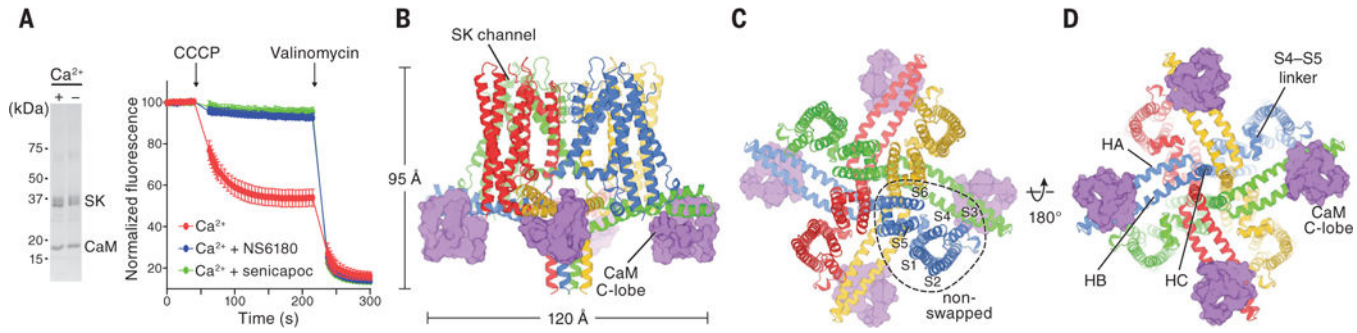

Fig. 1. Functional characterization and architecture of the Ca^{2+}-free SK-CaM channel complex.

(**A**) Purified SK-CaM channel complex and fluorescence-based liposome flux assay. Left, SK-CaM complex in the presence or absence of Ca^{2+} (2 mM $CaCl_2$ or 5 mM EGTA), analyzed by SDS-PAGE. Right, SK-CaM complex-mediated flux. Fluorescence changes due to K^+ flux were monitored over time (mean ± SEM; n = 4 to 8). Proteoliposomes in the presence of 2 mM $CaCl_2$ showed robust flux, which can be blocked by 10 μM NS6180 or senicapoc. CCCP, carbonyl cyanide m-chlorophenylhydrazone. (**B** to **D**) Cryo-EM structure of the Ca^{2+}-free SK-CaM complex. Each channel subunit is shown in a different color. Purple, CaM C-lobe in surface representation.

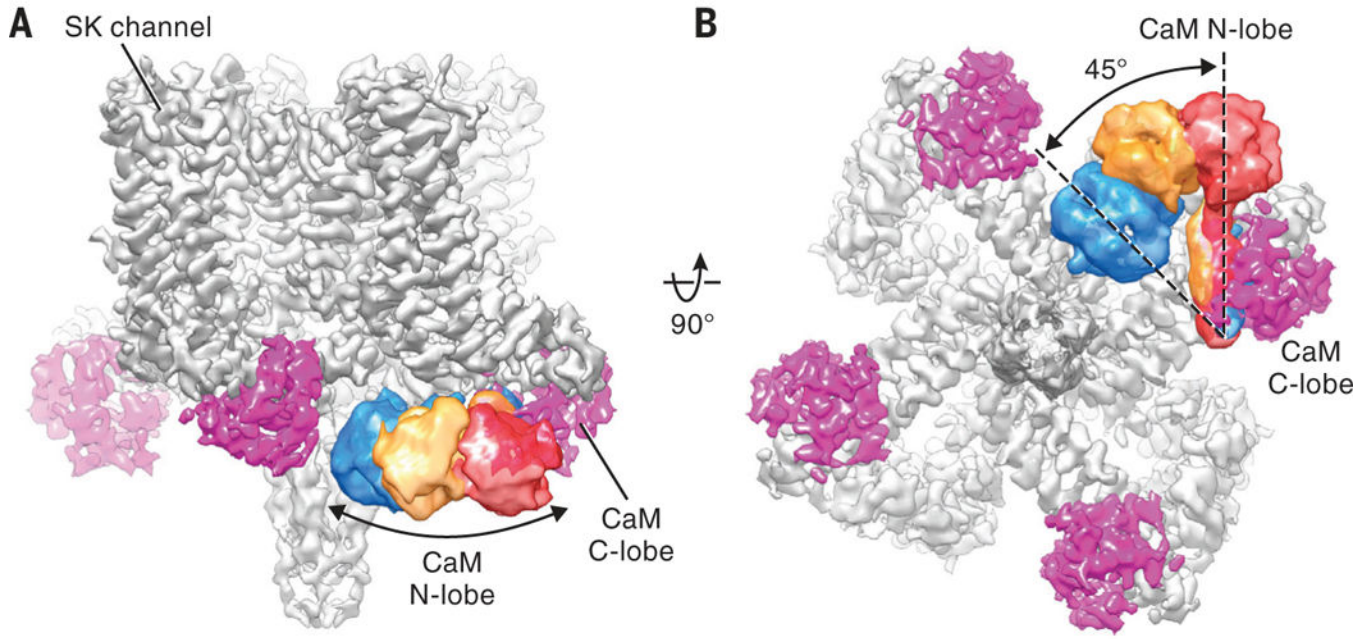

Fig. 2. Conformational dynamics of CaM N-lobe.

(**A** and **B**) Cryo-EM reconstruction of the Ca^{2+}-free SK-CaM complex. CaM N-lobe densities (blue, yellow, and red) from three classes after focused classification are superimposed on the consensus 3.4-Å resolution map.

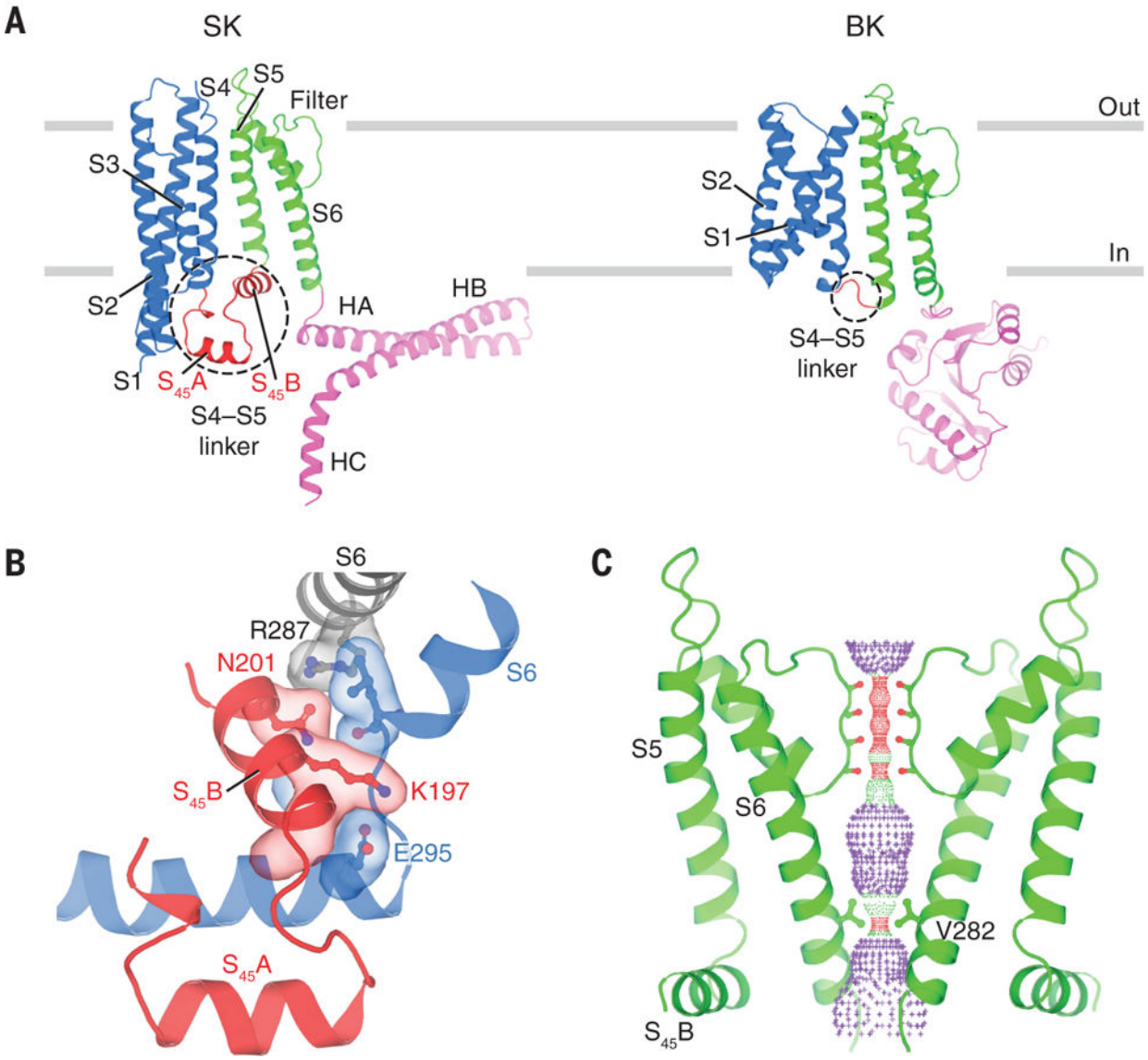

Fig. 3. Transmembrane domain and ion channel pore.

(**A**) Comparison of single SK and BK subunits. Gray bars represent approximate boundaries of the membrane bilayer. For clarity, only part of the BK intracellular domain is shown (Protein Data Bank ID, 5TJI). (**B**) Interface between $S_{45}B$ and S6 helices shown in surface representation. Gray, S6 helix from the same subunit as $S_{45}B$. Blue, S6 and HA helices from an adjacent subunit. (**C**) Channel pore with only two subunits shown for clarity. Pore radius: red, <1.15 Å; green, 1.15 to 2.30 Å; purple, >2.30 Å. Throughout the figures, single-letter abbreviations for the amino acid residues are as follows: A, Ala; C, Cys; D, Asp; E, Glu; G, Gly; I, Ile; K, Lys; L, Leu; N, Asn; Q, Gln; R, Arg; S, Ser; T, Thr; V, Val; and Y, Tyr.

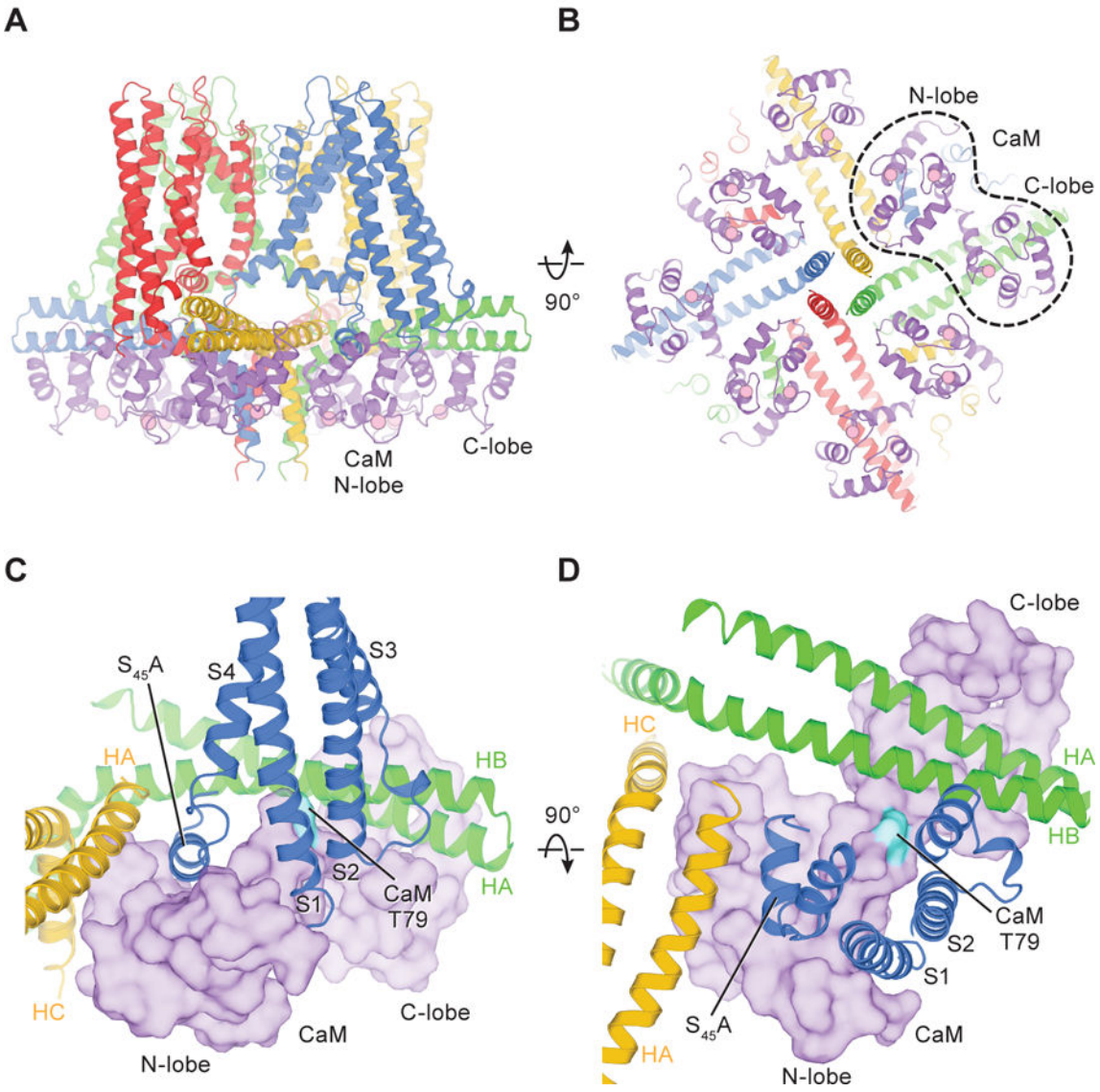

Fig. 4. Structure of the Ca^{2+}-bound SK-CaM channel complex.

(**A** and **B**) Structure of the Ca^{2+}-bound SK-CaM channel complex, colored as in Fig. 1 (purple, CaM). Ca^{2+} ions are shown as pink spheres. (**C** and **D**) Interactions between CaM (surface representation) and SK subunits.

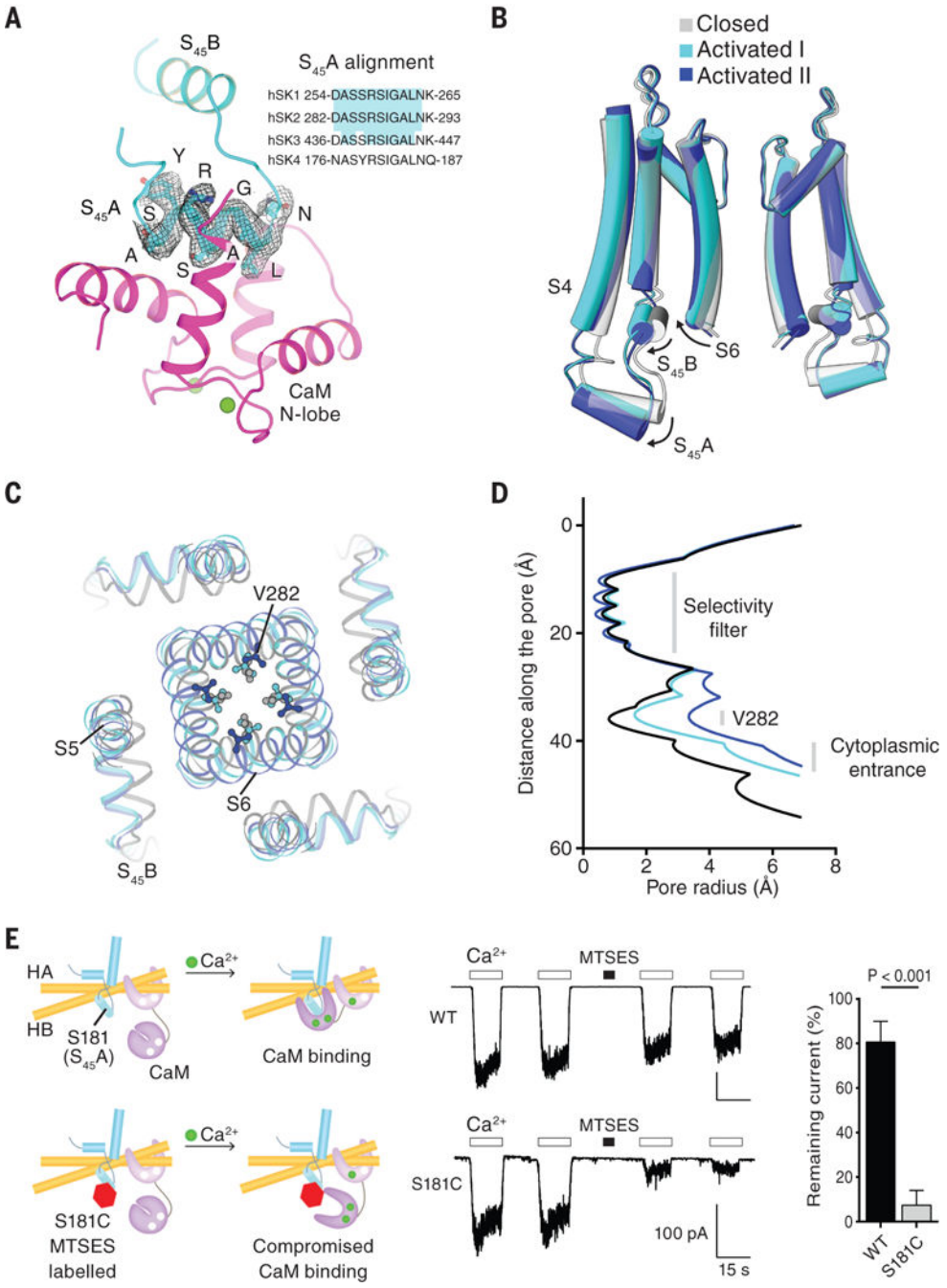

Fig. 5. Channel activation by Ca^{2+}-bound CaM.

(**A**) Binding of CaM N-lobe to SK $S_{45}A$. The cryo-EM density of $S_{45}A$ is shown (from the 3.5-Å resolution map of the Ca^{2+}-bound SK-CaM complex). Ca^{2+} ions are shown as green spheres. Inset, the amino acid sequence alignment of $S_{45}A$ from four human SK channel subtypes. The region highlighted in cyan is absolutely conserved. (**B**) Conformational changes in the S4–S5 linker and pore upon CaM N-lobe binding. Structures of different states are aligned at the selectivity filter. (**C**) Top-down view of conformational changes in the pore, shown from the extracellular side. (**D**) Radius of the pore in the activated states

versus the closed state. The radius is plotted as a function of the distance along the pore axis. V282 defines the narrowest constriction site of the cytoplasmic gate. (**E**) Preventing channel activation by compromising the CaM N-lobe–S_{45}A interaction. 10 μM Ca^{2+} or 2 mM MTSES was applied as indicated. Quantification of remaining currents after MTSES labeling is also shown (mean ± SD; n = 4 to 5, Student's *t* test). WT, wild type.

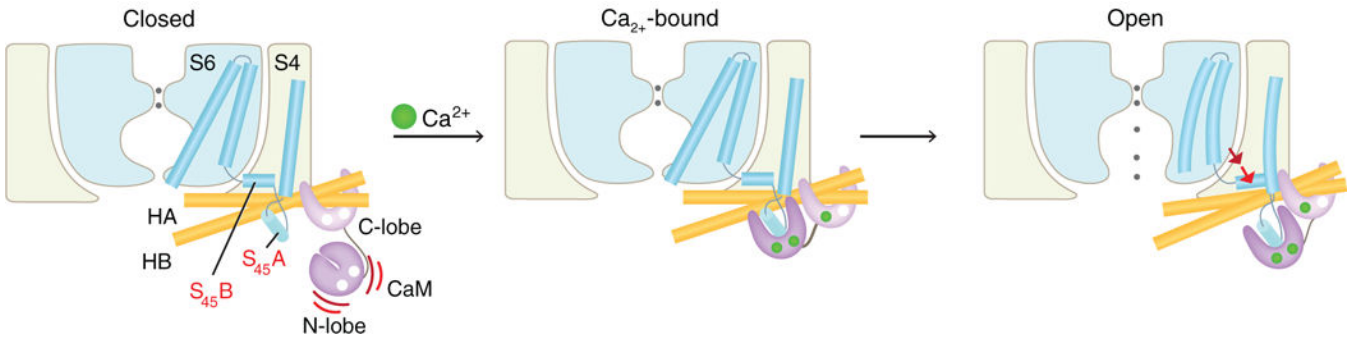

Fig. 6. Gating mechanism of the SK channel.

In the absence of Ca^{2+} (left panel), the SK channel is closed. The CaM C-lobe stays associated with the channel, whereas the CaM N-lobe barely binds to the channel. The very flexible N-lobe can adopt multiple conformations, but its binding pocket remains closed (60, 61). When Ca^{2+} binds to the CaM N-lobe (middle panel), the lobe rearranges into a more open conformation, allowing it to interact with $S_{45}A$. The N-lobe pulls the $S_{45}A$ helix downward, which displaces $S_{45}B$ away from the pore axis (right panel). This expands the S6 helical bundle and eventually opens the pore.